An improved local radial point interpolation method for transient heat conduction analysis*

Wang Feng(王 峰)[a)†], Lin Gao(林 皋)[a)], Zheng Bao-Jing(郑保敬)[b)], Hu Zhi-Qiang(胡志强)[a)]

[a)] *Faculty of Infrastructure Engineering, Dalian University of Technology, Dalian* 116024, *China*
[b)] *School of Aeronautics and Astronautics, Dalian University of Technology, Dalian* 116024, *China*

(Received 16 September 2012; revised manuscript received 10 January 2013)

The smoothing thin plate spline (STPS) interpolation using the penalty function method according to the optimization theory is presented to deal with transient heat conduction problems. The smooth conditions of the shape functions and derivatives can be satisfied so that the distortions hardly occur. Local weak forms are developed using the weighted residual method locally from the partial differential equations of the transient heat conduction. Here the Heaviside step function is used as the test function in each sub-domain to avoid the need for a domain integral. Essential boundary conditions can be implemented like the finite element method (FEM) as the shape functions possess the Kronecker delta property. The traditional two-point difference method is selected for the time discretization scheme. Three selected numerical examples are presented in this paper to demonstrate the availability and accuracy of the present approach comparing with the traditional thin plate spline (TPS) radial basis functions.

Keywords: thin plate splines, transient heat conduction, penalty function method, local radial point interpolation method

PACS: 02.60.–x, 02.60.Pn, 44.10.+i **DOI:** 10.1088/1674-1056/22/6/060206

1. Introduction

Transient heat transfer problems can be encountered in many engineering applications, such as nuclear energy and petrochemical engineering. Nowadays numerical methods are mainly adopted to analyze these problems.[1] In the past few decades, the finite element method (FEM) and the boundary element method (BEM) have been well developed and have been successfully applied to transient heat conduction analysis.[2,3] However, there exist some shortcomings, for example, the mesh generation for discretizations of complicated structural geometries in these methods is far more time-consuming and burdensome. As an alternative to these methods, the meshless method has attracted much attention due to its flexibility and good convergence rate.[4–8]

The meshless method is a new numerical approach for solving the partial differential equation (PDE), which relies only on a set of scattered nodes in the problem domain, so it can prime handle the large deformation problem because there is no need for remeshing of the domain. Many scholars research the meshless method using different approximation methods of the field function, and the meshless method can be used to solve the heat conduction problem. The meshless local Petrov–Galerkin (MLPG) method based on the local weak form has been proposed and developed by Atluri and his colleagues.[9–11] The MLPG method is a truly meshless method, as it does not require a mesh, either for the construction of the shape function, or for the integration of the local sub-domain, and has been successfully applied to solving heat conduction problems.[12–15] Though the MLPG method is an efficient meshless method, it is difficult to enforce the essential boundary conditions since the shape function constructed by the moving least-squares (MLS) approximation lacks the delta function property.[16] In order to solve this problem, Wang[17,18] proposed the radial point interpolation method (RPIM) using the radial basis functions (RBF) based on the point interpolation method (PIM) which was presented by Liu.[19,20] Cheng[21] extended the RPIM by incorporating with the local boundary integral equation method (LBIE). Dai[22,23] combined the moving Kriging interpolation with the MLPG method to solve the potential problems and solids problems.

Thin plate spline (TPS) which is one type of RBF, can be applied to the meshless method.[24] Though TPS has a more simple and concise functional form than the multi-quadrics (MQ) and Gaussian radial basis functions (Exp), it is rarely used. Brown[25] and Wang[26] applied TPS to non-rigid image alignment and found the selected points with large errors producing distortions. So they suggested weakening the effect of the constraint conditions using the penalty function method in order to achieve the tradeoff of warp smoothness and interpolation. Under the condition of regular nodes arrangement, a large amount of numerical experiments show that the smooth

*Project supported by the Key Program of the National Natural Science Foundation of China (Grand No. 51138001), the China–German Cooperation Project (Grand No. GZ566), the Innovative Research Groups Funded by the National Natural Science Foundation of China (Grand No. 51121005), and the Special Funds for the Basic Scientific Research Expenses for the Central University (Grant No. DUT13LK16).

†Corresponding author. E-mail: wangfengdut@gmail.com

© 2013 Chinese Physical Society and IOP Publishing Ltd

condition of the shape functions and derivatives which are obtained from the higher-order TPS cannot be satisfied and distortions occur, while the shape functions and derivatives got from the low-order TPS are nice but the nodes arrangement must be close in order to get an accurate solution. Here we use the penalty function method based on the optimization theory to improve TPS interpolation so that smoothing thin plate spline (STPS) radial basis functions are obtained, and the shape functions can have reliable smoothness. The parameters of the shape functions increase from one to two.

In this paper, a local radial point interpolation method (LRPIM) based on STPS interpolation is developed to perform the transient heat conduction analysis, and the Heaviside step function is used as the test function. The discrete equations are obtained using the local weak form of the partial differential equations (PDEs) derived from the weighted residual method. Three numerical examples are presented to verify the validity and accuracy of the proposed scheme in comparison with the traditional TPS radial basis functions.

2. Point interpolation using smoothing thin plate splines

2.1. Thin plate splines

Thin plate splines were introduced to geometric design by Duchon[27] by minimizing the integral that represents the bending energy of a surface. A thin plate spline is a physically motivated two-dimensional (2D) interpolation scheme for arbitrarily spaced tabulated data $(x_i, y_i, f(x_i, y_i))$. These splines are the generalization of the natural cubic splines in the one-dimensional (1D) case.

In two dimensions, one should choose a function $f(x)$ which exactly interpolates the data point (x_i, y_i), i.e., $y_i = f(x_i)$, and minimizes the functional penalty function $J(f)$

$$J(f) = \iint_{R^2} (f_{xx}^2 + 2f_{xy}^2 + f_{yy}^2)\,\mathrm{d}x\mathrm{d}y. \tag{1}$$

In fact, this is an optimization problem. Mathematically, it can be expressed as

$$\begin{aligned} &\min J(f) \\ &\text{s.t. } h_j(f) = y_j - f(x_j) = 0, j = 1, \ldots, q. \end{aligned} \tag{2}$$

The minimizing function of the form is

$$f(x,y) = \sum_{i=1}^{q} a_i R_i(x,y) + b_0 + b_1 x + b_2 y = \boldsymbol{R}_0 \boldsymbol{a} + \boldsymbol{P}_m \boldsymbol{b}, \tag{3}$$

where $R_i(x,y) = r_i^{\eta}$, η is the parameter of the shape function.

$$\boldsymbol{R}_0 = \begin{bmatrix} R_1(r_1) & R_2(r_1) & \cdots & R_q(r_1) \\ R_1(r_2) & R_2(r_2) & \cdots & R_q(r_2) \\ \vdots & \vdots & \ddots & \vdots \\ R_1(r_q) & R_2(r_q) & \cdots & R_q(r_q) \end{bmatrix}_{q\times q}, \tag{4}$$

$$\boldsymbol{P}_m^{\mathrm{T}} = \begin{bmatrix} 1 & 1 & \cdots & 1 \\ x_1 & x_2 & \cdots & x_q \\ \vdots & \vdots & \ddots & \vdots \\ p_m(\boldsymbol{x}_1) & p_m(\boldsymbol{x}_2) & \cdots & p_m(\boldsymbol{x}_q) \end{bmatrix}_{m\times q}. \tag{5}$$

An orthogonality condition that comes from the functional analysis is

$$\boldsymbol{P}_m^{\mathrm{T}} \boldsymbol{a} = 0. \tag{6}$$

2.2. Smoothing thin plate splines

The derivation of thin plate splines is a strictly constraint problem. However, the thin plate spline interpolation is sensitive to the deviation of points so that the singularity occurs in constructing the shape functions and derivatives of meshless methods easily. Therefore, the penalty function method is employed to change the constraint problem into the unconstraint problem in order to weaken the constraint condition according to the optimization theory.[28] Interestingly, this process can not only reduce the effect of deviation but also improve the smoothing characteristics of the shape functions and derivatives. The corresponding penalty function is

$$\begin{aligned} &F(f,\lambda) = \frac{1}{q}\sum_{j=1}^{q} h_j^2(f) + \lambda J(f) \\ &\min F(f,\lambda), \end{aligned} \tag{7}$$

where λ is a fixed smoothing parameter. The smoothing parameter λ controls the separation of signal and noise. If $\lambda = 0$, the function f exactly interpolates the data, implying zero noise. If λ is very large, the function f approaches a hyperplane.

The approximate solution of Eq. (2) can be obtained by solving Eq. (7). The following form can be obtained

$$f(x,y) = (\boldsymbol{R}_0 + q\lambda \boldsymbol{I})\boldsymbol{a} + \boldsymbol{P}_m \boldsymbol{b}, \tag{8}$$

where $\boldsymbol{I}$ is a $q \times q$ identity matrix. The condition for Eq. (6) is also satisfied.

The λ that corresponds to the spline function f can be accurately estimated by minimizing the generalized cross validation (GCV),[29,30] given by

$$\frac{1}{q}\frac{(\boldsymbol{y} - \boldsymbol{A}(\lambda)\boldsymbol{y})^{\mathrm{T}}(\boldsymbol{y} - \boldsymbol{A}(\lambda)\boldsymbol{y})}{(\mathrm{tr}(\boldsymbol{I} - \boldsymbol{A}(\lambda))/q)^2}, \tag{9}$$

where $\boldsymbol{A}(\lambda)$ is the matrix which transforms the vector of data values into the vector of predicted values, and thus

$$\hat{\boldsymbol{y}} = \boldsymbol{A}(\lambda)\boldsymbol{y}, \tag{10}$$

where $\hat{\boldsymbol{y}}$ is the vector of predicted values and $\boldsymbol{A}(\lambda)$ is the influence matrix.

2.3. The construction of the shape function

Considering a function $u(\boldsymbol{x})$ defined in the domain Ω which is discretized by a set of scattered nodes $\boldsymbol{x}_1,\ldots,\boldsymbol{x}_N$ and then the discretized function values of $u(\boldsymbol{x})$ can be defined as $\{u_i = u(\boldsymbol{x}_i)\}_{i=1}^N$. Now, for any local sub-domain $\Omega_x \subseteq \Omega$, the field function can be approximated by

$$\boldsymbol{u}^h(\boldsymbol{x}) = \sum_{i=1}^{n} R_i(\boldsymbol{x})a_i + \sum_{j=1}^{m} p_j(\boldsymbol{x})b_j = \boldsymbol{R}^{\mathrm{T}}(\boldsymbol{x})\boldsymbol{a} + \boldsymbol{p}^{\mathrm{T}}(\boldsymbol{x})\boldsymbol{b}, \tag{11}$$

where $R_i(\boldsymbol{x})$ is the TPS function, n is the number of nodes in the local support domain of $\boldsymbol{x}$. $p_j(\boldsymbol{x})$ are monomial basis functions in the space coordinate $\boldsymbol{x}^{\mathrm{T}} = [x,y]$, m is the number of polynomial basis functions and the coefficients a_i and b_j are interpolation constants.

In TPS, the variable is only the distance r between the interpolation point $\boldsymbol{x}$ and a node $\boldsymbol{x}_i$. For a two-dimensional (2D) problem, r is defined as

$$r = \sqrt{(x-x_i)^2 + (y-y_i)^2}. \tag{12}$$

The following linear polynomial basis is used

$$\boldsymbol{p}^{\mathrm{T}}(\boldsymbol{x}) = \{1\ x\ y\}. \tag{13}$$

In order to determine the constants a_i and b_j, Eq. (8) is enforced to be satisfied at these n nodes in the local support domain and can be rewritten in a matrix form as

$$\boldsymbol{u} = (\boldsymbol{R}_0 + N\lambda\boldsymbol{I})\boldsymbol{a} + \boldsymbol{P}_m\boldsymbol{b} \tag{14}$$

with m constraint conditions

$$\boldsymbol{P}_m^{\mathrm{T}}\boldsymbol{a} = 0, \tag{15}$$

where the vector of function values $\boldsymbol{u}$ is

$$\boldsymbol{u}^{\mathrm{T}} = \{u_1\ u_2\ u_3\ \cdots\ u_n\}. \tag{16}$$

The moment matrix of TPS is

$$\boldsymbol{R}_0 = \begin{bmatrix} R_1(r_1) & R_2(r_1) & \cdots & R_n(r_1) \\ R_1(r_2) & R_2(r_2) & \cdots & R_n(r_2) \\ \vdots & \vdots & \ddots & \vdots \\ R_1(r_n) & R_2(r_n) & \cdots & R_n(r_n) \end{bmatrix}_{n\times n}. \tag{17}$$

The polynomial moment matrix is

$$\boldsymbol{P}_m^{\mathrm{T}} = \begin{bmatrix} 1 & 1 & \cdots & 1 \\ x_1 & x_2 & \cdots & x_n \\ \vdots & \vdots & \ddots & \vdots \\ p_m(\boldsymbol{x}_1) & p_m(\boldsymbol{x}_2) & \cdots & p_m(\boldsymbol{x}_n) \end{bmatrix}_{m\times n}. \tag{18}$$

The vector of unknown coefficients for TPS is

$$\boldsymbol{a}^{\mathrm{T}} = \{a_1\ a_2\ \cdots\ a_n\}. \tag{19}$$

The vector of unknown coefficients for polynomial is

$$\boldsymbol{b}^{\mathrm{T}} = \{b_1\ b_2\ \cdots\ b_m\}. \tag{20}$$

In Eq. (17), r_k in $R_i(r_k)$ is

$$r_k = \sqrt{(x_k - x_i)^2 + (y_k - y_i)^2}. \tag{21}$$

Combining Eqs. (14) and (15) yields the following set of equations in the matrix form

$$\begin{bmatrix} \boldsymbol{R}_0 + N\lambda\boldsymbol{I} & \boldsymbol{P}_m \\ \boldsymbol{P}_m^{\mathrm{T}} & \boldsymbol{0} \end{bmatrix} \begin{Bmatrix} \boldsymbol{a} \\ \boldsymbol{b} \end{Bmatrix} = \begin{Bmatrix} \boldsymbol{u} \\ \boldsymbol{0} \end{Bmatrix}. \tag{22}$$

By solving Eq. (22), the solution for coefficients $\boldsymbol{a}$ and $\boldsymbol{b}$ is

$$\begin{aligned} \boldsymbol{b} &= \boldsymbol{S}_b\boldsymbol{u}, \\ \boldsymbol{a} &= \boldsymbol{S}_a\boldsymbol{u}, \end{aligned} \tag{23}$$

where

$$\begin{aligned} \boldsymbol{S}_b &= \left[\boldsymbol{P}_m^{\mathrm{T}}(\boldsymbol{R}_0 + N\lambda\boldsymbol{I})^{-1}\boldsymbol{P}_m\right]^{-1}\boldsymbol{P}_m^{\mathrm{T}}(\boldsymbol{R}_0 + N\lambda\boldsymbol{I})^{-1}, \\ \boldsymbol{S}_a &= (\boldsymbol{R}_0 + N\lambda\boldsymbol{I})^{-1}(\boldsymbol{I} - \boldsymbol{P}_m\boldsymbol{S}_b). \end{aligned} \tag{24}$$

Equation (11) can be rewritten as

$$\begin{aligned} u^h(\boldsymbol{x}) &= [\boldsymbol{R}^{\mathrm{T}}(\boldsymbol{x})\boldsymbol{S}_a + \boldsymbol{p}^{\mathrm{T}}(\boldsymbol{x})\boldsymbol{S}_b]\boldsymbol{u} \\ &= \boldsymbol{\Phi}(\boldsymbol{x})\boldsymbol{u} = \sum_{k=1}^{n} \varphi_k(\boldsymbol{x})u_k, \end{aligned} \tag{25}$$

where

$$\varphi_k(\boldsymbol{x}) = \sum_{i=1}^{n} R_i(\boldsymbol{x})S_{aik} + \sum_{j=1}^{m} p_j(\boldsymbol{x})S_{bjk}. \tag{26}$$

The partial derivatives of the shape functions can be easily obtained as

$$\begin{aligned} \varphi_{k,x} &= \frac{\partial\varphi_k(\boldsymbol{x})}{\partial x} = \sum_{i=1}^{n}\frac{\partial R_i}{\partial x}S_{aik} + \sum_{j=1}^{m}\frac{\partial p_j}{\partial x}S_{bjk}, \\ \varphi_{k,y} &= \frac{\partial\varphi_k(\boldsymbol{x})}{\partial y} = \sum_{i=1}^{n}\frac{\partial R_i}{\partial y}S_{aik} + \sum_{j=1}^{m}\frac{\partial p_j}{\partial y}S_{bjk}. \end{aligned} \tag{27}$$

2.4. Correlation parameter versus shape functions

Considering a rectangular domain $\Omega = [0,1]\times[0,1]$ in two dimensions with 25 (5×5) regularly distributed nodes. η and λ are correlation parameters versus the shape functions. When choosing $\eta = 3$ and $\lambda = 3.5\times10^{-4}$, the shape functions and the first-order derivatives are evaluated at the point $(0.5,\ 0.5)$ as shown in Fig. 1 and Fig. 2.

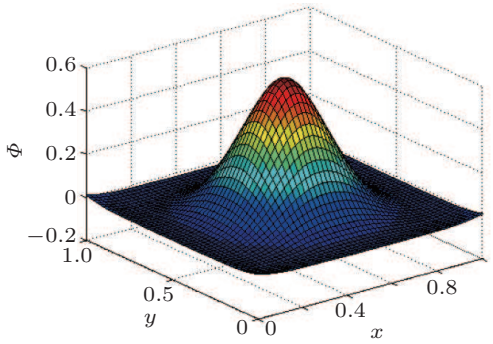


Fig. 1. (color online) The shape functions.

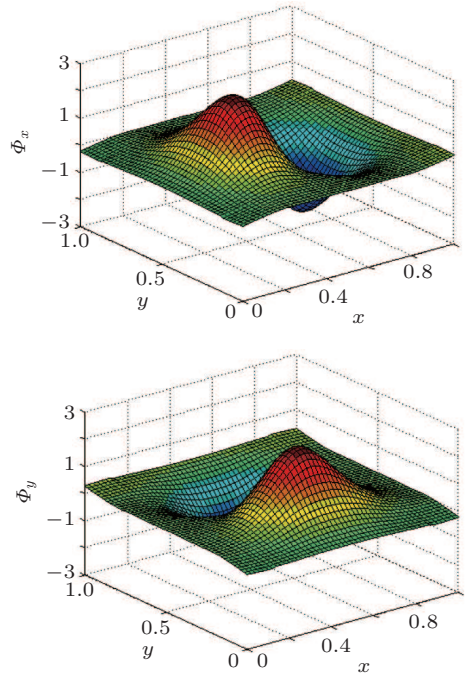


Fig. 2. (color online) The first-order derivatives of the shape function.

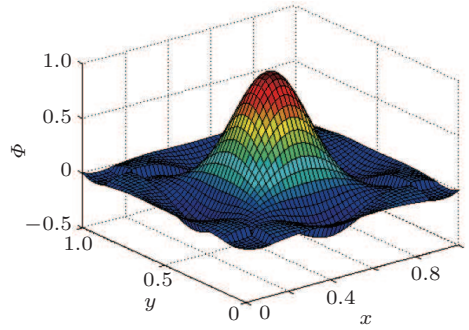


Fig. 3. (color online) The shape functions.

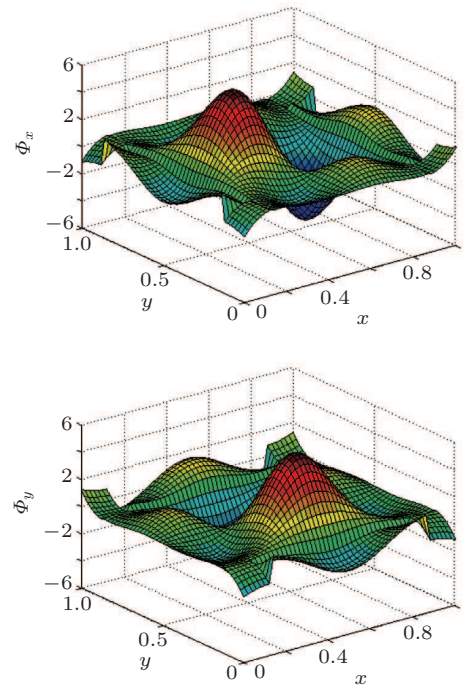


Fig. 4. (color online) The first-order derivatives of the shape function.

The shape functions and the first-order derivatives resulting from traditional TPS are evaluated at the point $(0.5,\ 0.5)$ when η equals 6.001. The results are shown in Fig. 3 and Fig. 4.

Compared with the traditional TPS interpolation, the improved shape functions and derivatives have better smoothness and definition.

3. The formulation of LRPIM for transient heat conduction problems

The transient heat conduction equation belongs to the parabolic partial differential equations. Let us consider the transient heat problem for two dimensions in the domain Ω bounded by Γ and the governing equation is given by

$$\rho c\frac{\partial T}{\partial t}-\frac{\partial}{\partial x}\left(k_x\frac{\partial T}{\partial x}\right)-\frac{\partial}{\partial y}\left(k_y\frac{\partial T}{\partial y}\right)-Q=0 \quad \text{in } \Omega. \tag{28}$$

The boundary conditions for this problem can be obtained by any combination of the following types

$$T-\bar{T}=0 \ \text{ on } \ \Gamma_1, \tag{29}$$

$$k_x\frac{\partial T}{\partial x}n_x+k_y\frac{\partial T}{\partial y}n_y=\bar{q} \ \text{ on } \ \Gamma_2, \tag{30}$$

$$k_x\frac{\partial T}{\partial x}n_x+k_y\frac{\partial T}{\partial y}n_y-h(T_a-T)=0 \ \text{ on } \ \Gamma_3, \tag{31}$$

where Γ_1, Γ_2, Γ_3 denote the Dirichlet, Neumann, and Robin boundary conditions, respectively. T represents the temperature field. t is time. ρ and c are the density and specific heat, respectively. Q is the density of heat sources. k_x and k_y are the coefficients of the heat conduction along x and y directions. n_x and n_y are the direction cosines of the outward normal to the boundary surface. $\bar{T}$, $\bar{q}$, and h are the prescribed temperature, the prescribed heat flux, the prescribed heat transfer coefficient on boundaries Γ_1, Γ_2, and Γ_3, respectively.

The initial condition is

$$T(x,y,0)=T_0(x,y), \tag{32}$$

where T_0 is the initial temperature.

3.1. Local weak forms of the transient heat conduction problems

The local weak form of Eq. (28) over a local sub-domain Ω_s bounded by Γ_s, can be written as

$$\int_{\Omega_s} v\left[\rho c\frac{\partial T}{\partial t}-\frac{\partial}{\partial x}\left(k_x\frac{\partial T}{\partial x}\right)-\frac{\partial}{\partial y}\left(k_y\frac{\partial T}{\partial y}\right)-Q\right]\mathrm{d}\Omega=0, \tag{33}$$

where v is the test function.

Using the divergence theorem, Eq. (33) can be integrated by parts to become

$$\int_{\Omega_s}\left(\rho c\frac{\partial T}{\partial t}v+k_x\frac{\partial T}{\partial x}\frac{\partial v}{\partial x}+k_y\frac{\partial T}{\partial y}\frac{\partial v}{\partial y}-vQ\right)\mathrm{d}\Omega$$

$$-\int_{\Gamma_s} v\left(k_x\frac{\partial T}{\partial x}n_x+k_y\frac{\partial T}{\partial y}n_y\right)\mathrm{d}\Gamma=0. \tag{34}$$

When an intersection exists between the local boundary Γ_s and the global boundary Γ, the boundary Γ_s is comprised of four parts: the internal boundary Γ_{sI}, the Dirichlet boundary Γ_{s1}, the Neumann boundary Γ_{s2}, and the Robin boundary Γ_{s3}. If no intersection exists between the local boundary Γ_s and the global boundary Γ, $\Gamma_{sI}=\Gamma_s$ and the integrals over Γ_{s1}, Γ_{s2}, Γ_{s3} vanish.

Substituting Eqs. (30) and (31) into Eq. (34), we obtain

$$\begin{aligned}&\int_{\Omega_s}\left(\rho c\frac{\partial T}{\partial t}v+k_x\frac{\partial T}{\partial x}\frac{\partial v}{\partial x}+k_y\frac{\partial T}{\partial y}\frac{\partial v}{\partial y}-vQ\right)\mathrm{d}\Omega\\&-\int_{\Gamma_{sI}} v\left(k_x\frac{\partial T}{\partial x}n_x+k_y\frac{\partial T}{\partial y}n_y\right)\mathrm{d}\Gamma\\&-\int_{\Gamma_{s1}} v\left(k_x\frac{\partial T}{\partial x}n_x+k_y\frac{\partial T}{\partial y}n_y\right)\mathrm{d}\Gamma\\&-\int_{\Gamma_{s2}} v\bar{q}d\Gamma-\int_{\Gamma_{s3}} vh(T_a-T)\mathrm{d}\Gamma=0.\end{aligned} \tag{35}$$

The Heaviside step function is chosen as the test function v in this research

$$v=\begin{cases}1, & x\in\Omega_s,\\ 0, & x\notin\Omega_s.\end{cases} \tag{36}$$

The local weak form (35) is transformed into the following simple boundary integral equation

$$\begin{aligned}&\int_{\Omega_s}\rho c\frac{\partial T}{\partial t}\mathrm{d}\Omega-\int_{\Gamma_{sI}}\left(k_x\frac{\partial T}{\partial x}n_x+k_y\frac{\partial T}{\partial y}n_y\right)\mathrm{d}\Gamma\\&-\int_{\Gamma_{s1}}\left(k_x\frac{\partial T}{\partial x}n_x+k_y\frac{\partial T}{\partial y}n_y\right)\mathrm{d}\Gamma+\int_{\Gamma_{s3}}hT\,\mathrm{d}\Gamma\\&=\int_{\Omega_s}Q\mathrm{d}\Omega+\int_{\Gamma_{s2}}\bar{q}\mathrm{d}\Gamma+\int_{\Gamma_{s3}}hT_a\mathrm{d}\Gamma.\end{aligned} \tag{37}$$

An arbitrary shape support domain can be used and a circle or rectangular support domain is commonly used in 2D problems.

3.2. Discretization and the time difference scheme

For the transient heat conduction, the temperature field function relates to not only the space coordinate but also time t. Because the shape functions are independent of time, the temperature field function can be expressed as

$$T(\boldsymbol{x},t)=\sum_{k=1}^{n}\varphi_k(\boldsymbol{x})T_k(t). \tag{38}$$

Substituting Eq. (38) into Eq. (37), the following discrete equation for all nodes can be obtained

$$\boldsymbol{C}\dot{\boldsymbol{T}}(t)+\boldsymbol{K}\boldsymbol{T}(t)=\boldsymbol{F}(t), \tag{39}$$

where

$$\begin{aligned}\boldsymbol{C}_{IJ}&=\int_{\Omega_s}\rho c\varphi_J(\boldsymbol{x})\mathrm{d}\Omega,\\ \boldsymbol{K}_{IJ}&=-\int_{\Gamma_{sI}}\left[k_x\frac{\partial\phi_J(\boldsymbol{x})}{\partial x}n_x+k_y\frac{\partial\phi_J(\boldsymbol{x})}{\partial y}n_y\right]\mathrm{d}\Gamma\\&\quad-\int_{\Gamma_{s1}}\left[k_x\frac{\partial\phi_J(\boldsymbol{x})}{\partial x}n_x+k_y\frac{\partial\phi_J(\boldsymbol{x})}{\partial y}n_y\right]\mathrm{d}\Gamma+\int_{\Gamma_{s3}}h\phi_J(\boldsymbol{x})\mathrm{d}\Gamma,\end{aligned} \tag{40, 41}$$

$$\boldsymbol{F}_I=\int_{\Omega_s}Q\mathrm{d}\Omega+\int_{\Gamma_{s2}}\bar{q}\mathrm{d}\Gamma+\int_{\Gamma_{s3}}hT_a\mathrm{d}\Gamma. \tag{42}$$

Equation (39) is a set of ordinary differential equations with respect to time. Here we adopt the traditional two-point difference technique for time discretization

$$\theta\left(\frac{\partial T}{\partial t}\right)_{t+\Delta t}+(1-\theta)\left(\frac{\partial T}{\partial t}\right)_t=\frac{T_{t+\Delta t}-T_t}{\Delta t}, \tag{43}$$

where θ satisfies the condition $0\le\theta\le1$. When $\theta=0$, it is the forward Euler difference scheme. When $\theta=1$, it is the backward Euler difference scheme. When $\theta=1/2$, it is the CN (Crank–Nicolson) scheme. When $\theta=2/3$, it is the Galerkin scheme. We use the CN scheme to solve Eq. (39). Substituting Eq. (43) into Eq. (39) results in

$$\left(\frac{\bar{K}_{t+\Delta t}}{2}+\frac{C}{\Delta t}\right)T_{t+\Delta t}=\frac{1}{2}\left(\bar{F}_{t+\Delta t}+\bar{F}_t\right)+\left(\frac{C}{\Delta t}-\frac{\bar{K}_t}{2}\right)T_t. \tag{44}$$

4. Numerical examples

For the purpose of the error estimation, the Sobolev norms are defined as follows:

$$\|u\|=\left(\int_\Omega u^2\mathrm{d}\Omega\right)^{1/2}. \tag{45}$$

The relative errors are defined as

$$e_\mathrm{r}=\frac{\|u^\mathrm{num}-u^\mathrm{exact}\|}{\|u^\mathrm{exact}\|}. \tag{46}$$

For a node x_i, there are two local independent domains: the support domain Ω_x (size r_s) and the interpolation domain Ω_i (size r_i), which are defined as $r_s=\alpha d_i$ and $r_i=\beta d_i$, respectively. α and β are coefficients and d_i is the average distance among the nodes of the local sub-domain.

4.1. The transient heat field in the square domain

Considering a square domain

$$\Omega=\{(x,y),0\le x\le\pi\ \mathrm{m},\ \ 0\le y\le\pi\ \mathrm{m}\}, \tag{47}$$

with

$$k_x=k_y=1\ \mathrm{W/(m\cdot{}^\circ C)},\quad \rho c=1\ \mathrm{J/(m^3\cdot{}^\circ C)}, \tag{48}$$

$Q=0\ ^\circ\mathrm{C}$ because of no internal heat source. The boundary conditions and the initial temperature for this transient heat conduction problem are as follows:

$$T(0,y,t)=T(x,0,t)=T(\pi,y,t)=T(x,\pi,t)=0, \tag{49}$$

$$T(x,y,0)=10\sin(x)\sin(y),\quad (x,y)\in\Omega, \tag{50}$$

where $T(x,y,t)$ is the temperature at the point coordinate (x,y) at any given time t. The corresponding analytical solution for this problem is

$$T(x,y,t)=10\sin(x)\sin(y)\,\mathrm{e}^{-2t}. \tag{51}$$

In this study, the coefficients are $\alpha = 1.85$ and $\beta = 0.5$. As shown in Fig. 5, the regular (Fig. 5(a)) and irregular (Fig. 5(b)) node distributions of 11×11 are employed. $\eta = 3$ and $\lambda = 7.2 \times 10^{-5}$ are chosen in constructing the shape functions. The time step in CN is $\Delta t = 0.02$ s.

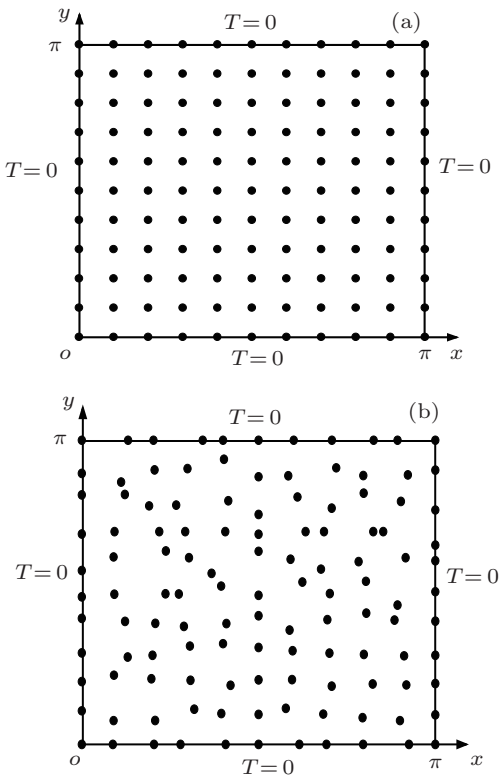


Fig. 5. (a) Regularly distributed 121 nodes and (b) irregularly distributed 121 nodes.

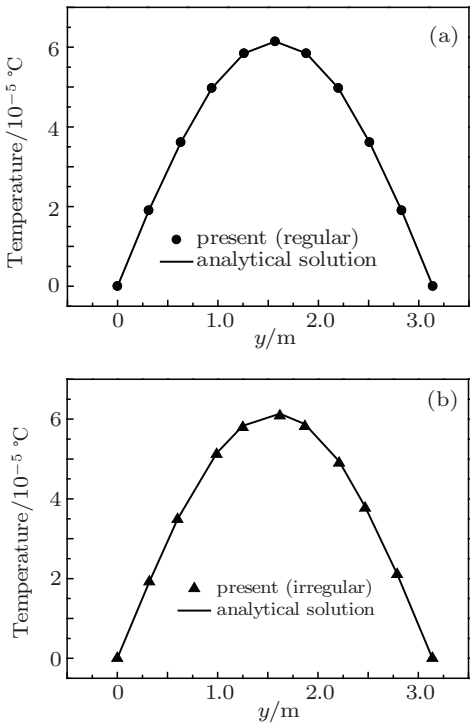


Fig. 6. The temperature distributions along $x = \pi/2$ m at $t = 6$ s for regular (a) and irregular (b) cases.

The computation temperature distribution along $x = (\pi/2)$ m at $t = 6$ s by using the present method is shown in Fig. 6 for both regular (Fig. 6(a)) and irregular (Fig. 6(b)) cases. It can be easily observed that a very nice agreement is achieved between the numerical results and the analytical solutions at these two cases with different nodal distributions. Figure 7 shows the variations of the temperature on point A $(\pi/2, \pi/2)$ in 6 seconds for regular (Fig. 7(a) and irregular (Fig. 7(b)) cases. It can clearly demonstrate that irregular node distribution does not affect much numerical accuracy in this meshless method.

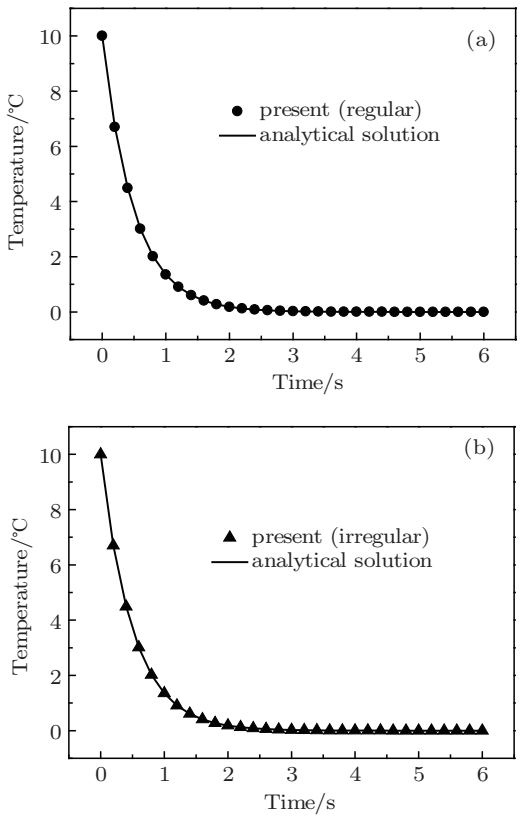


Fig. 7. The variations of temperature on point A for regular (a) and irregular (b) cases.

As shown in Table 1, the present meshless method derived from the STPS interpolation is a very effective method in comparison with the traditional TPS RPIM. Although the traditional TPS RPIM ($\eta = 6.001$) can get an accurate solution, the shape functions and derivatives produce distortions. In the meantime, the traditional TPS RPIM ($\eta = 3.001$) needs more nodes to be assigned and it is time-comsuming.

Table 1. The relative errors and computational time of meshless methods.

Meshless method	Relative errors/%	Computational time/s	Nodes distribution
Present method (regular)	0.17	2.597	11×11
Present method (irregular)	0.73	2.442	11×11
Traditional TPS ($\eta = 6.001$)	0.55	2.577	11×11
Traditional TPS ($\eta = 3.001$)	2.63	2.641	11×11
Traditional TPS ($\eta = 3.001$)	0.70	10.595	19×19

4.2. The transient heat field in the cubic domain

As shown in Fig. 8, the cube is 20-mm long, 10-mm high, and has unit thickness. The initial temperature $T_0 = 20$ °C has been assumed and there is no heat source in the domain. Then heat the cube in some medium whose temperature is maintained at $T_a = 100$ °C. The top and bottom boundary surfaces are insulated. The prescribed heat transfer coefficients of the left and right boundary surfaces are $h = 1600$ W/(m$^2\cdot$°C). $k_x = k_y = 16$ W/(m$\cdot$°C), $\rho c = 10^6$ J/(m$^3\cdot$°C) are assumed in the calculation and 231 nodes are employed to model the domain. It can be simplified to the plane problems.

Parameters selected for the present method in this example are $\Delta t = 0.01$ s, $\alpha = 3.5$, $\beta = 0.5$. $\eta = 3$, and $\lambda = 3.8 \times 10^{-5}$. Due to the symmetry, only the the temperature distribution of $x > 0$ needs to be determined. The computational results at time $t = 1$ s, 2 s, 3 s located at point A (0, 0), B (5, 5), and C (10, 0) are presented in Table 2, respectively. Also shown in the table are the computational results obtained from the finite element software ANSYS.

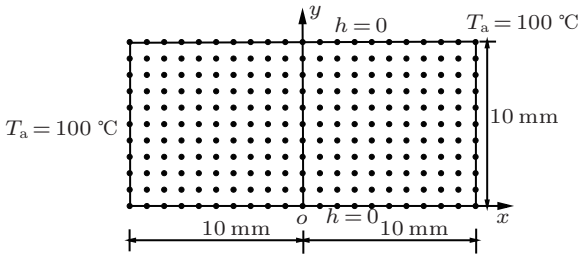


Fig. 8. Node distribution with 231 nodes.

Table 2. The comparison of the temperature obtained from some kinds of numerical methods.

Time/s	Point	FEM/°C	The present method	
			Computational results/°C	Relative error/%
1	*A*	22.356	22.331	0.11
	B	27.421	27.475	0.20
	C	46.278	46.364	0.19
2	*A*	29.623	29.659	0.12
	B	35.721	35.770	0.14
	C	53.633	53.669	0.07
3	*A*	37.259	37.313	0.14
	B	42.930	42.977	0.11
	C	59.023	59.045	0.04

As expected, the present numerical solutions are very close to the results obtained from the finite element software ANSYS. This example confirms that the developed method in this paper can give a good numerical solution indeed.

4.3. The transient heat field in a square plate with a circular hole

Consider a square plate with a central circular hole: $x^2 + y^2 \le a^2$ (a is the radius of the hole). The boundary around the circular hole is insulated and the other boundaries are prescribed with a heat flux $\bar{q} = 10$ W/m^2. Due to the symmetry, only one quarter of the plate is considered as shown in Fig. 9. For this transient heat conduction problem, the material parameters are as follows: $k_x = k_y = 1$ W/(m$\cdot$°C), $\rho c = 1$ J/(m$^3\cdot$°C). The plate has zero initial temperature and there is no heat source in the domain.

The node arrangement for the square plate with a central hole is shown in Fig. 10 and the domain is discretized by 225 nodes in computation. The parameters are taken as $\Delta t = 0.01$ s, $\alpha = 2.4$, $\beta = 0.5$. $\eta = 3$, and $\lambda = 1.7 \times 10^{-5}$ for this example.

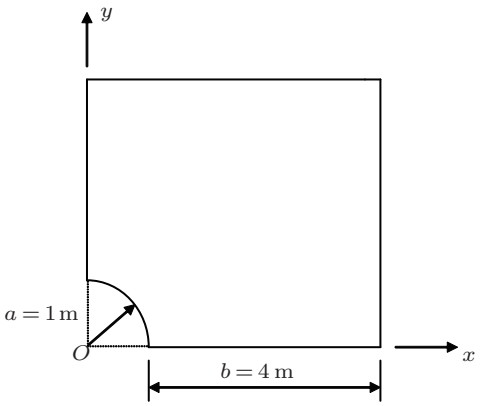


Fig. 9. The square plate with a central hole based on fourfold symmetry.

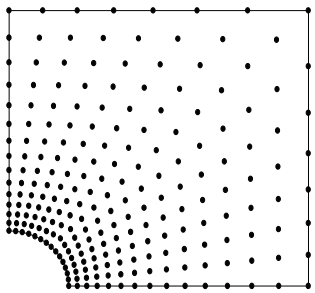


Fig. 10. Node distribution in the plate with a central hole.

The present numerical results of temperature at time $t =$

2 s along y axis are compared with the finite element solutions computed from the software ANSYS. It can be seen from Fig. 11 that the present method can give a good numerical solution indeed.

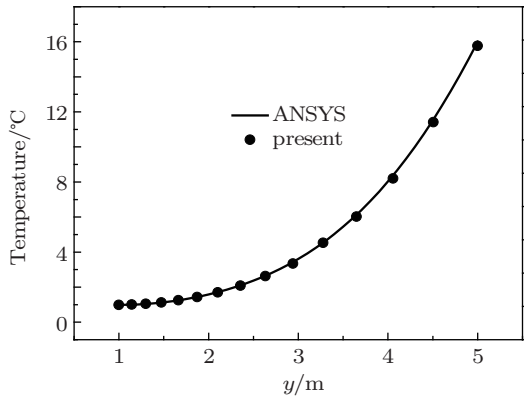


Fig. 11. Temperature at the section $x = 0$ of the square plate with a hole.

5. Conclusion

This paper presents and develops the LRPIM using the Heaviside step function as the test function to solve transient heat conduction problems. Because the smoothing thin plate spline (STPS) interpolation using the penalty function method can achieve the tradeoff of warp smoothness and interpolation, the LRPIM employs the STPS interpolation to construct the shape functions and derivatives. The essential boundary conditions can be implemented like the classical FEM as the shape functions used in this paper possess the Kronecker delta property. The LRPIM avoids the need for the domain integral and the traditional CN difference method is selected for the time discretization scheme. The computational results demonstrate that the present method based on the STPS interpolation is an effective meshless method.

References

[1] Minkowycz W J, Sparrow E M, Schneider G E and Pletcher R H 2006 *Handbook of Numerical Heat Transfer*, 2nd edn. (New York: John Wiley & Sons)
[2] Wilson E L and Nickell R E 1966 *Nucl. Eng. Des.* **4** 276
[3] Dargush G F and Banerjee P K 1991 *Int. J. Numer. Meth. Eng.* **31** 1231
[4] Belytschko T, Krongauz Y, Organ D, Fleming M and Krysl P 1996 *Comp. Meth. Appl. Mech. Eng.* **139** 3
[5] Zhang X, Liu Y and Ma S 2009 *Adv. Mech.* **39** 1 (in Chinese)
[6] Cheng R J and Cheng Y M 2007 *Acta Phys. Sin.* **56** 5569 (in Chinese)
[7] Cheng R J and Cheng Y M 2007 *Acta Mech. Sin.* **39** 843 (in Chinese)
[8] Chen L and Cheng Y M 2008 *Acta Phys. Sin.* **57** 6047 (in Chinese)
[9] Atluri S N, Kim H G and Cho J Y 1999 *Comput. Mech.* **24** 348
[10] Atluri S N and Zhu T 1998 *Comput. Mech.* **22** 117
[11] Atluri S N and Zhu T 2000 *Comput. Mech.* **25** 169
[12] Sladek J, Sladek V, Tan C L and Atluri S N 2008 *Comput. Model. Eng. Sci.* **32** 161
[13] Sladek J, Sladek V and Hon Y C 2006 *Eng. Anal. Bound. Elem.* **30** 650
[14] Chen L and Liew K M 2011 *Comput. Mech.* **47** 455
[15] Li Q H, Chen S S and Kou G X 2011 *J. Comput. Phys.* **230** 2736
[16] Lancaster P and Salkauskas K 1981 *Math. Comput.* **37** 141
[17] Wang J G and Liu G R 2002 *Int. J. Numer. Meth. Eng.* **54** 1623
[18] Wang J G, Liu G R and Lin P 2002 *Int. J. Solids. Struct.* **39** 1557
[19] Liu G R and Gu Y T 2001 *Int. J. Numer. Meth. Eng.* **50** 937
[20] Liu G R and Gu Y T 2001 *J. Sound. Vib.* **246** 29
[21] Dai B D and Cheng Y M 2007 *Acta Phys. Sin.* **56** 597 (in Chinese)
[22] Zheng B J and Dai B D 2010 *Acta Phys. Sin.* **59** 5182 (in Chinese)
[23] Zheng B J and Dai B D 2011 *Appl. Math. Comput.* **218** 563
[24] Liu G R, Zhang G Y, Gu Y T and Wang Y Y 2005 *Comput. Mech.* **36** 421
[25] Brown B J and Rusinkiewicz S 2004 *Proceedings of the 2nd International Symposium on 3D Data Processing, Visualization and Transmission*, September 6–9, 2004, Thessaloniki, Greece, p. 759
[26] Liu R H, Wang B L and Huang X Y 2009 *China Digital Medicine* **4** 19
[27] Duchon J 1977 *Proceedings of a Conference Held at Oberwolfach*, April 25–May 1, 1976, Oberwolfach, Germany, p. 85
[28] Tang H W and Qin Z X 2004 *Practical Methods of Optimization*, 3rd edn. (Dalian: Dalian University of Technology Press) p. 158 (in Chinese)
[29] Craven P and Wahba G 1979 *Numer. Math.* **31** 377
[30] Hancock P A and Hutchinson M F 2006 *Environ. Modell. Softw.* **21** 1684